J. Non-Newtonian Fluid Mech. 160 (2009) 47–54

Contents lists available at ScienceDirect

Journal of Non-Newtonian Fluid Mechanics

journal homepage: www.elsevier.com/locate/jnnfm

Velocity overshoots in gradual contraction flows

Robert J. Poole [a], Manuel A. Alves [b,*]

[a] Department of Engineering, University of Liverpool, Brownlow Street, Liverpool L69 3GH, United Kingdom
[b] Departamento de Engenharia Química, CEFT, Faculdade de Engenharia, Universidade do Porto, Rua Dr. Roberto Frias, 4200-465 Porto, Portugal

ARTICLE INFO

Article history:
Received 29 July 2008
Received in revised form 10 March 2009
Accepted 12 March 2009

Keywords:
Viscoelastic flow in gradual contractions
Cat's ears
UCM model
PTT model
Creeping flow
Finite-volume method

ABSTRACT

This study reports the results of a systematic numerical investigation, using the upper-convected Maxwell (UCM) and Phan-Thien–Tanner (PTT) models, of viscoelastic fluid flow through three-dimensional gradual planar contractions of various contraction ratios with the aim of investigating experimental observations of extremely large near-wall velocity overshoots in similar geometries [R.J. Poole, M.P. Escudier, P.J. Oliveira, Laminar flow of a viscoelastic shear-thinning liquid through a plane sudden expansion preceded by a gradual contraction, Proc. Roy. Soc. Lond. Ser. A 461 (2005) 3827]. We are able to obtain good qualitative agreement with the experiments, even using the UCM model in creeping-flow conditions, showing that neither inertia, second normal-stress difference nor shear-thinning effects are required for the phenomenon to be observed. Guided by the numerical results we propose a simple explanation for the occurrence of the velocity overshoots and the conditions under which they arise.

1. Introduction

Experimental velocity measurements of the flow of a high-molecular weight flexible polymer solution through planar *gradual* contraction–sudden expansion geometries [1,2] have revealed an interesting fluid-dynamic effect. Spanwise[1] profiles of the streamwise velocity in the *XZ*-centreplane exhibited extreme velocity overshoots close to the sidewalls, up to three times the centreline velocity in magnitude, that due to their appearance were called "cat's ears". More recent experiments, without the sudden expansion component, have confirmed that the appearance of the "cat's ears" profiles are a sole consequence of the smooth contraction [3]. Representative velocity profiles are reproduced in Fig. 1(a), together with a schematic of the contraction geometry used in the experiments, in which a representative velocity profile along the spanwise (neutral) direction is illustrated (Fig. 1(b)).

Three-dimensional viscoelastic calculations using the Phan-Thien–Tanner (PTT) model [4] have been attempted to match the experimental conditions of Ref. [2] with a few limited simulations reported in Poole et al. [2] and an extended systematic study reported in Afonso and Pinho [5]. Although some modest success in predicting velocity overshoots was achieved, the magnitude of the overshoots – at most about 10% higher than the centreline velocity – was always much lower than that observed in the experiments. To capture these weak overshoots the full PTT model was required ($\xi \neq 0$ producing $N_2 \neq 0$ in steady simple shear flow) together with strong strain hardening (low values of ε) and some inertia. In these simulations it was speculated that the presence of the geometric singularity due to the sudden expansion prevented convergence at higher Deborah numbers and that, if convergence could be achieved, a non-zero second normal-stress difference may not be required for the effect to be observed (i.e. $\xi \neq 0$ just allowed the *De*–*Re* space to be reached where "cat's ears" occur).

Our interest in the current study is to revisit the problem in an attempt to capture the extreme nature of the "cat's ears" effect and to try to reveal the mechanism for their appearance. To do so our approach, in contrast to the simulations of Refs. [2,5], is to concentrate on modelling a gradual contraction section alone, as in the recent experiments of Keegan et al. [3]. Furthermore we set aside the goal of trying to exactly match the experimental conditions of Refs. [1,2] by selecting a related, but simplified, 3D-geometry and by varying the *Re* and *De* numbers in a systematic way. Using such a methodology we are able to show that, even for the rheologically "simple" UCM model, extreme velocity overshoots can be predicted even in the absence of inertia, i.e. the velocity overshoots are a purely *elastic* effect. Thus "cat's ears" profiles appear to be an inherent feature of viscoelastic flow through gradual contractions provided certain conditions, which we identify based on our numerical results, are satisfied.

The rest of this paper is organised as follows; in Section 2 we briefly describe the equations to be solved, the numerical method, the geometry and the meshes used; in Section 3 we discuss the

* Corresponding author. Fax: +351 225081449.
E-mail addresses: robpoole@liv.ac.uk (R.J. Poole), mmalves@fe.up.pt (M.A. Alves).

[1] Here we use the terms streamwise for the flow (x) direction and spanwise for the neutral (z) direction.

0377-0257/$ – see front matter © 2009 Elsevier B.V. All rights reserved.
doi:10.1016/j.jnnfm.2009.03.005

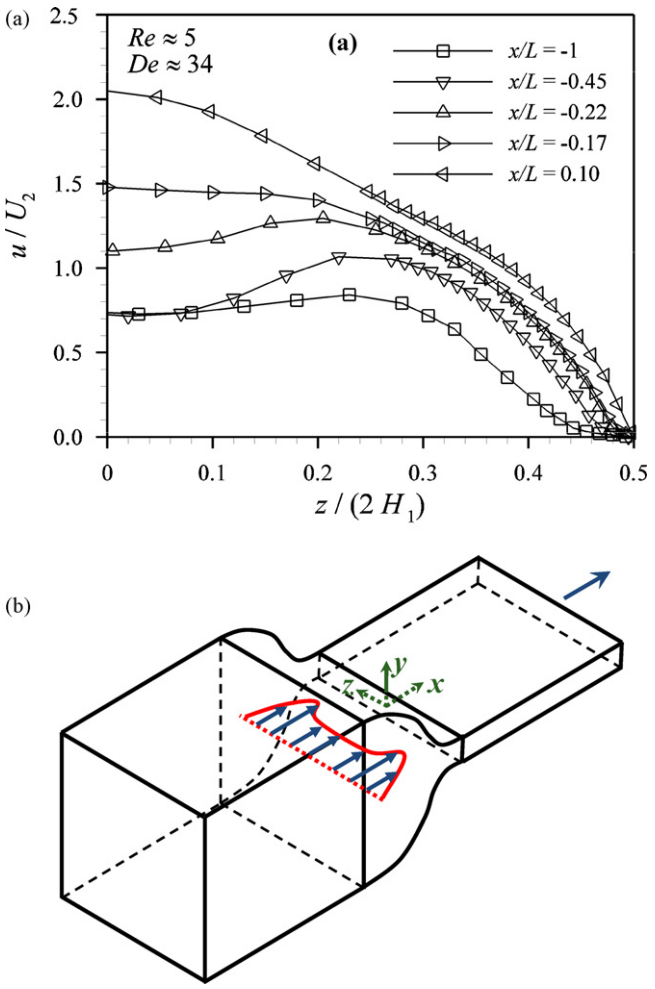

Fig. 1. (a) Spanwise profiles of the streamwise velocity for an aqueous solution of 3000 ppm polyacrylamide in an 8:1 planar gradual contraction flow $Re \approx 5$, $De \approx 34$ (adapted from Ref. [3]) and (b) schematic of the geometry and coordinate axis.

results for a Newtonian fluid followed by the results of the viscoelastic models in Section 4; in Section 5, based on our numerical results, we discuss a possible mechanism for the "cat's ears" effect before summarising our findings in Section 6.

2. Governing equations, numerical method, geometry and computational meshes

We are concerned with the isothermal flow of an incompressible viscoelastic fluid through a gradual three-dimensional planar contraction geometry. The equations to solve are those of conservation of mass:

$$\nabla \cdot \boldsymbol{u} = 0, \tag{1}$$

and of momentum:

$$\rho \left[\frac{\partial \boldsymbol{u}}{\partial t} + \boldsymbol{u} \cdot \nabla \boldsymbol{u} \right] = -\nabla p + \nabla \cdot \boldsymbol{\tau}. \tag{2}$$

For reasons of rheological simplicity most of the simulations we report here are for the well known upper-convected Maxwell (UCM) model [6]; in addition some simulations are conducted for the simplified version of the Phan-Thien and Tanner model (PTT) [4] of

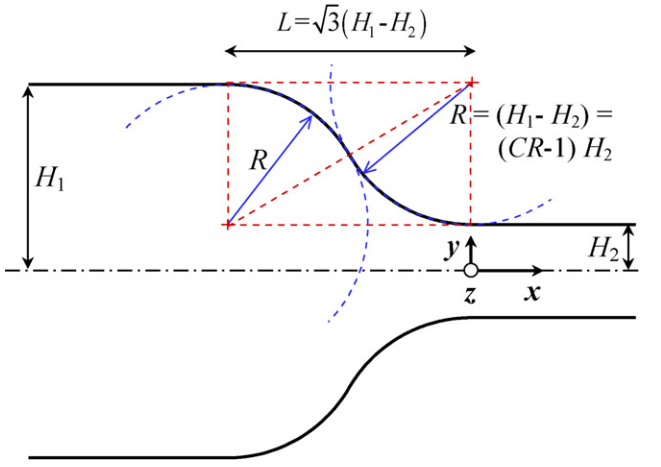

Fig. 2. Schematic of planar gradual contraction geometry. The depth of the geometry in the z-direction is constant ($2H_1$) (adapted from Ref. [10]).

which the UCM is a limiting case:

$$\lambda \left[\frac{\partial \boldsymbol{\tau}}{\partial t} + \nabla \cdot \boldsymbol{u}\boldsymbol{\tau} \right] + f(\mathrm{Tr}\,\boldsymbol{\tau})\boldsymbol{\tau} = \eta_p(\nabla \boldsymbol{u} + \nabla \boldsymbol{u}^{\mathrm{T}}) + \lambda(\boldsymbol{\tau} \cdot \nabla \boldsymbol{u} + \nabla \boldsymbol{u}^{\mathrm{T}} \cdot \boldsymbol{\tau}). \tag{3}$$

Eq. (3) retains only the upper-convected part of the full Gordon-Schowalter derivative. In the current study the stress function $f(\mathrm{Tr}\,\boldsymbol{\tau})$ takes the linear form proposed in Ref. [4]:

$$f(\mathrm{Tr}\,\boldsymbol{\tau}) = 1 + \frac{\lambda\varepsilon}{\eta_p}\mathrm{Tr}(\boldsymbol{\tau}). \tag{4}$$

In Eqs. (3) and (4) the constant model parameters are the relaxation time of the polymer λ, the zero-shear polymer viscosity η_p and the extensibility parameter ε. Setting the ε parameter to zero produces the UCM model. The UCM model exhibits both a constant shear viscosity η and first normal-stress coefficient (and hence relaxation time) allowing us to explore the effects of elasticity without the complications of shear-thinning of either the shear viscosity or relaxation time. In contrast the PTT model exhibits shear-thinning of both these parameters but has the benefit of bounded extensional stresses in purely extensional flow enabling higher Deborah numbers to be reached.

A fully implicit finite-volume numerical method is used to solve Eqs. (1)–(4). The original numerical method, and subsequent developments, has been described in great detail in Refs. [7–9] and so is not unnecessarily repeated here.

The gradual contraction geometries we investigate here are essentially three-dimensional versions of the geometries we used to investigate the phenomenon of "divergent flow" in Ref. [10]. A schematic 2D projection of the geometry used in the numerical simulations is shown in Fig. 2. The geometry consists of two ducts, the larger (inlet) one being square in cross-section and having a half-height H_1 and the other (entrant) having the same width but different height ($2H_2$) connected by two arcs (one convex, the other concave) of constant radius of curvature, $R = H_1 - H_2$. Defining the contraction ratio as CR ($=H_1/H_2$) we can also express this radius of curvature as $R = (CR-1)H_2$. The coordinate system is set on the XY and XZ symmetry planes at the "entrance" to the smaller channel. Although not identical to the geometries used in Refs. [1–3], this choice enables consistency between geometries of differing contraction ratio and also a constant wall radius of curvature. Despite these small differences the essential nature of the experimental geometry used in Ref. [3] is maintained.

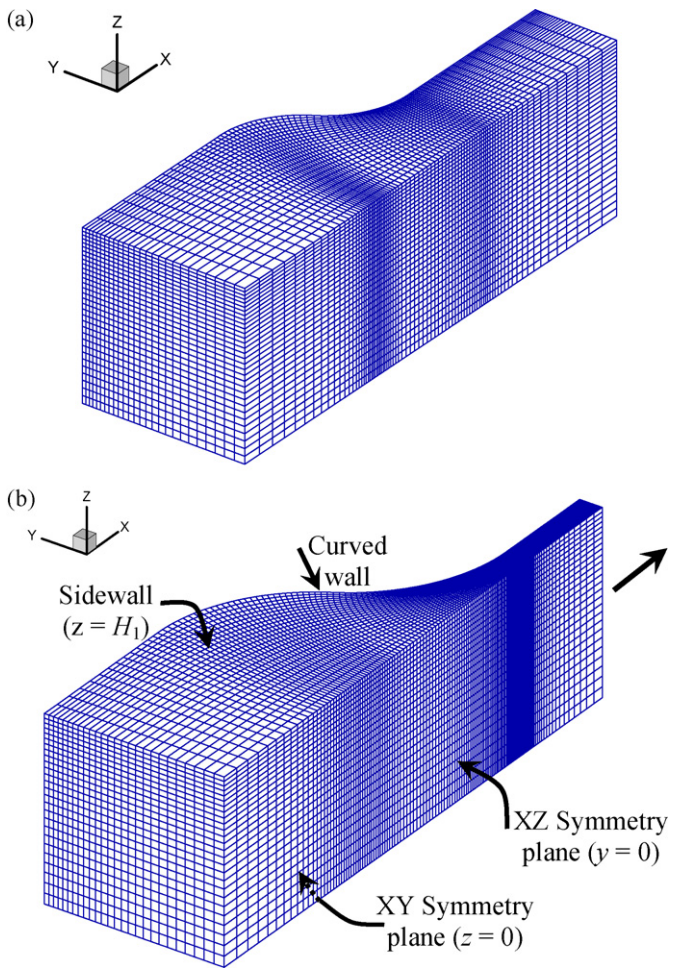

Fig. 3. Zoomed view of two representative computational meshes (a) $CR = 2$ (the region $-4 \le x/H_2 \le 2$ is shown) and (b) $CR = 8$ (the region $-20 \le x/H_2 \le 5$ is shown).

In the current problem the non-dimensional parameters of relevance for the UCM fluid flow are those of the Reynolds number ($\equiv \rho U_2 H_2/\eta$), the Deborah number which here we define based on downstream quantities, $De = \lambda U_2/H_2$, and the contraction ratio $CR = H_1/H_2$.

To study the effect of contraction ratio we investigated four different geometries of varying contraction ratio: $CR = 2$, 4, 8 and 16. The meshes used are structured and non-orthogonal, and were created in such a way that the cells are approximately aligned with the streamlines in the two-dimensional Newtonian case [10]. Due to the symmetry of the geometry only a quarter of the full domain is simulated with symmetry boundary conditions imposed at the *XY* and *XZ* symmetry planes. Typical meshes are shown in Fig. 3 and quantified in Table 1.

Table 1
Major characteristics of the computational meshes.

Mesh	*NC*	DOF	$\Delta x_{min}/H_2$	$\Delta y_{min}/H_2$	$\Delta z_{min}/H_2$
CR2	176 384	1 763 840	0.027	0.021	0.041
CR4	131 144	1 311 440	0.044	0.021	0.08
CR8	164 944	1 649 440	0.046	0.025	0.19
CR16	378 560	3 785 600	0.045	0.027	0.41

NC, number of cells; DOF, number of degrees of freedom; Δx_{min}, Δy_{min}, Δz_{min}, minimum cell sizes.

3. Newtonian simulations

In classical Newtonian fluid mechanics gradual contractions are, at least at relatively high contraction ratios, often used to produce "uniform" velocity profiles; the most obvious exploitation of which is in wind-tunnel design in aerodynamics [11,12], although they are also used in pipe-flow studies as inlet conditioners [13,14] and elsewhere [15].

Fig. 4 shows 3D contours of the velocity development in the *XZ*-centreplane for a modest contraction ratio (in this case $CR = 4$) for different Reynolds numbers. In order to quantify this flattening effect for different contraction ratios and Reynolds numbers it is useful to define a "flattening parameter" $\mathcal{F}$ which represents the spanwise extent over which the velocity is "two dimensional" at the end of the contraction section ($x = 0$) in the *XZ*-centreplane. We define "two dimensional" as being within 5% of the centreline velocity and we normalise with the width of the duct, such that $0 < \mathcal{F} < 1$. We plot this flattening parameter versus *Re* for various contraction ratios in Fig. 5.

As can be observed in Fig. 5 the flattening parameter increases with *Re*, although at *high* values of *Re* there is a reduction of $\mathcal{F}$, at least for low *CR* cases. This slight reduction is directly related with the increase of the development length as *Re* increases (see, e.g. Ref. [16]). Fig. 4, for $CR = 4$, and other results for different contraction ratios (not shown here for concision) clearly illustrate that the velocity profiles are monotonic along both the *x*- and *z*-directions. For creeping-flow conditions the flattening parameter can be estimated from the fully developed downstream velocity profile, since the velocity development length is small. Comparison between numerical simulations at $Re = 0.01$ and predictions from the theoretical fully developed velocity profiles agree to within 5% ($CR = 2$) and 2% ($CR = 16$).

The results illustrated in Figs. 4 and 5, obtained with Newtonian fluids, lead us to conclude that the onset of velocity undershoots/overshoots along the streamwise direction (which is typical of viscoelastic flows [10]), or along the *spanwise* direction (the "cat's ears" phenomenon) is related with viscoelastic effects, either alone or complemented by inertia and/or shear-thinning, as will be demonstrated in the next section.

4. Viscoelastic simulations

In order to identify the driving mechanism for the onset of "cat's ears", we undertook a systematic study of the influence of *De* and *CR* on the observed flow patterns and on the local spanwise velocity profiles within the contraction using the UCM model. In Fig. 6 we show the effect of *De* on the observed velocity profiles along the *XZ* centreplane for a *high* contraction ratio ($CR = 8$) and in Fig. 7 we present similar plots for a *low* contraction ratio ($CR = 2$). For the higher contraction ratio, one observes that viscoelasticity leads to a significant overshoot of the streamwise velocity along the centreline ($y = z = 0$), a behaviour typically observed in contraction and expansion flows of highly elastic fluids (e.g. Refs. [10,17]). In this high *CR* case no velocity overshoots along the spanwise direction ("cat's ears") are observed. However, for the case of low contraction ratios it can be observed that at high *De* streamwise velocity overshoots are present along the spanwise direction, which are stronger within the gradual contraction region. These velocity overshoots propagate from the lateral sidewalls towards the centre, until eventually they are smeared out by diffusion. For the Newtonian cases presented in Figs. 6 and 7, the velocity profiles have a similar behaviour to those illustrated in Fig. 4 for $CR = 4$.

These results show that the "cat's ears" phenomenon can be reproduced using the UCM model under creeping-flow conditions, thus demonstrating that this effect is purely elastic in nature. In order to quantify the intensity of the "cat's ears" for different con-

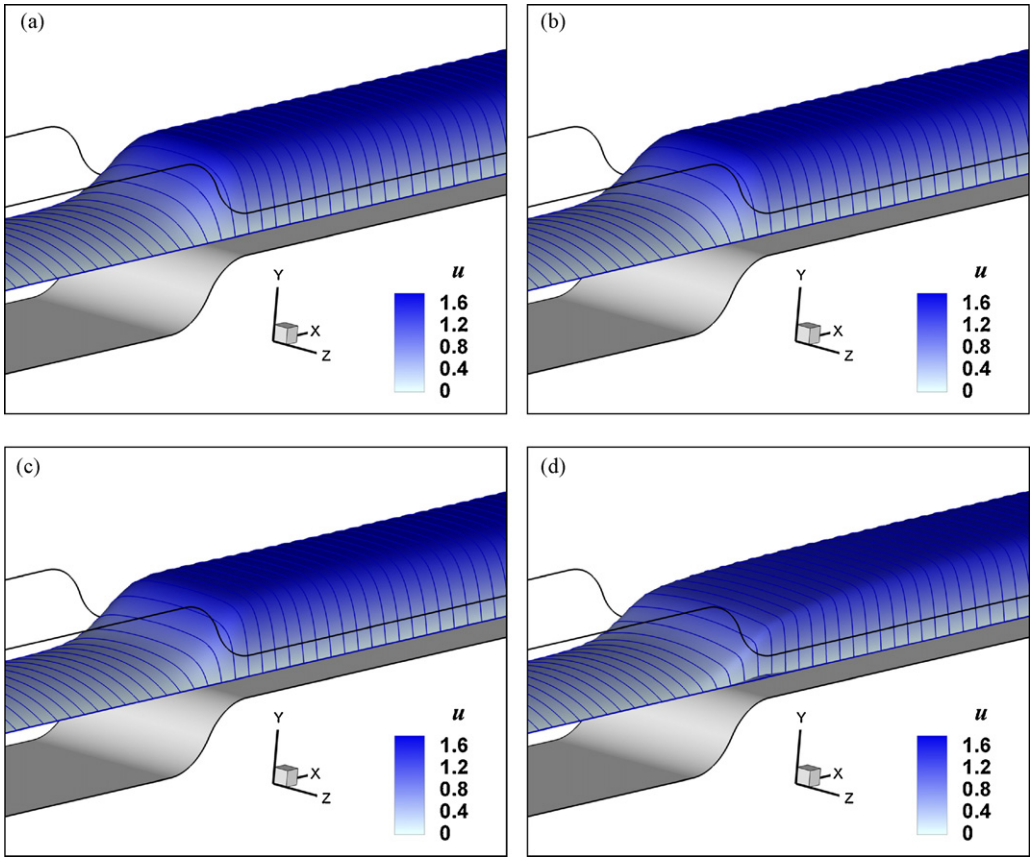

Fig. 4. Streamwise velocity profiles on the *XZ* centreplane ($y = 0$) for a Newtonian fluid at different Reynolds numbers for $CR = 4$: (a) $Re = 0$; (b) $Re = 1$; (c) $Re = 10$; (d) $Re = 100$. The streamwise velocity profiles represented as lines are at consecutive x-positions that are apart a distance of $\Delta x/H_2 = 1$.

traction ratios and Deborah numbers, we find it useful to define the following dimensionless parameter,

$$C = \max\left[\frac{u_{\max}(x, y = 0, z) - u_c(x, y = 0, z = 0)}{u_c(x, y = 0, z = 0)}\right], \tag{5}$$

where $u_{\max}$ represents the maximum streamwise velocity along the spanwise direction along the centreplane $y = 0$, at a constant streamwise position x, and u_c the centreline velocity ($y = z = 0$) at the same x-location. Thus C is a relative measure of spanwise velocity overshoots, with $C = 0$ for the Newtonian case devoid of such phenomena. In Fig. 8 we plot the C parameter for $CR = 2$, 4 and 8, as a function of the Deborah number, under creeping-flow conditions. We observe that the critical *De* for the onset of "cat's ears" increases approximately linearly with *CR*. It is also apparent that above the critical *De* the rate of increase of C decreases with *CR*, however for the higher contraction ratios only a limited range above the critical conditions is achieved before the flow looses steadiness. Therefore we cannot conclude that the "cat's ears" effect is a feature solely of low *CR* contractions, as might be expected from Figs. 6 and 7.

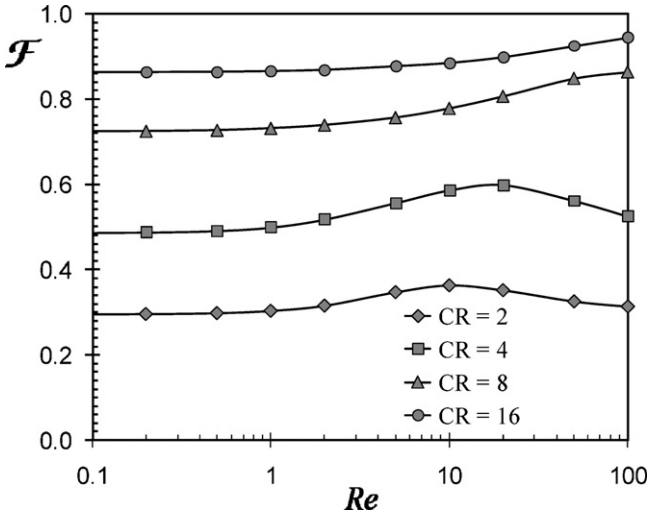

Fig. 5. Effect of *CR* and *Re* on "flattening parameter" for Newtonian fluid flow through gradual planar contractions.

The previous results demonstrate that it is possible to predict the "cat's ears" phenomenon without inertia. Nevertheless, the observed profiles in the experiments [1–3] are significantly more intense. In order to reproduce such extreme behaviour, we have conducted additional simulations for flow conditions where inertial effects are important, as is the case in the experiments. We varied the Reynolds number for different *De* cases, and, as a typical example, in Fig. 9 we show the velocity profiles for $CR = 4$ and a high Deborah number flow ($De = 6$) using the UCM model. Increasing inertial effects leads to significantly more intense "cat's ears", and the velocity profiles become even more complex downstream of the contraction region. However, for $Re \gtrsim 2$ a reduction of the velocity overshoots is observed, coupled with a delay of flow redevelopment. Interestingly for the highest *Re* a second velocity overshoot appears downstream of the end of the contraction.

Although the fluids used in the experiments [1–3] all have shear-thinning characteristics, to a greater or lesser extent dependent on concentration, the simulations with the UCM model demonstrate that shear-thinning is not a necessary condition for the onset of strong "cat's ears". Nevertheless, we have also performed additional simulations using the linear form of the PTT model (i.e. Eqs. (3) and (4)) in order to demonstrate that it is not necessary to use models that exhibit unbounded behaviour under strong extensional flow,

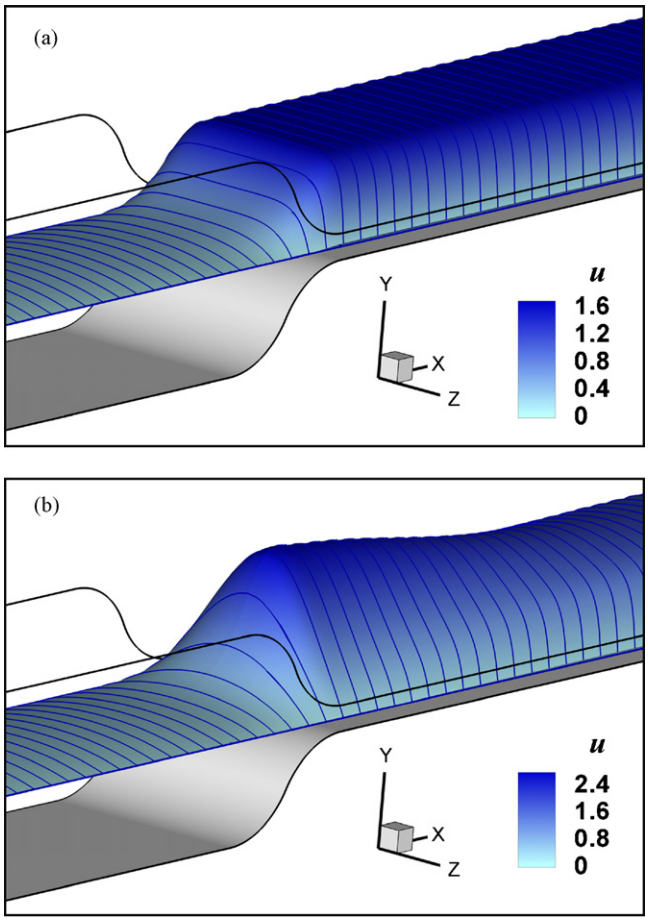

Fig. 6. Streamwise velocity profiles in the *XZ* centreplane ($y = 0$) under creeping-flow conditions for $CR = 8$ for (a) Newtonian fluid and (b) UCM fluid at $De = 12$. The streamwise velocity profiles – represented as lines – are at consecutive x-positions that are apart a distance of $\Delta x/H_2 = 2$.

Fig. 7. Streamwise velocity profiles in the *XZ* centreplane ($y = 0$) under creeping-flow conditions for $CR = 2$ for (a) Newtonian fluid and (b) UCM fluid at $De = 5$. The streamwise velocity profiles – represented as lines – are at consecutive x-positions that are apart a distance of $\Delta x/H_2 = 0.5$.

such as the UCM model, to capture the "cat's ears" effect. We note that the UCM model only exhibits an unbounded extensional viscosity under steady-state extensional flow. In a contraction flow the fluid is subjected to a finite extension, and therefore the normal stresses (and extensional viscosity) under purely extensional flow (along the centreline) are always bounded (for details cf. Ref. [10]).

For the PTT model we selected an extensibility parameter $\varepsilon = 0.02$, which is typical of dilute polymeric solutions (such as some of those fluids used in the experiments of Refs. [1–3]). In Fig. 10 we present the velocity profiles predicted along the streamwise direction along the plane $y = 0$, illustrating that a substantial velocity overshoot in the centreline is observed, a behaviour typical of highly elastic flows in contraction geometries (although in this case the overshoot is significantly more intense than has been observed in these flows hitherto). Again, we also observe the emergence of considerable "cat's ears" in the smooth contraction region, further demonstrating that this elastic phenomenon is a "landmark" feature of highly elastic smooth contraction flows. In the next section we describe a simple mechanism to explain qualitatively the driving force that leads to the appearance of the velocity overshoots for highly elastic flows.

5. Origin of "cat's ears" phenomena

From the foregoing it is clear that the "cat's ears" phenomenon is due to elastic effects and can be predicted under creeping-flow conditions. Although, as we have shown, inertia enhances the phenomenon, we will restrict the present analysis to creeping flow of constant shear-viscosity fluids. However it can be expected that the underlying mechanism remains the same regardless of the level of inertia.

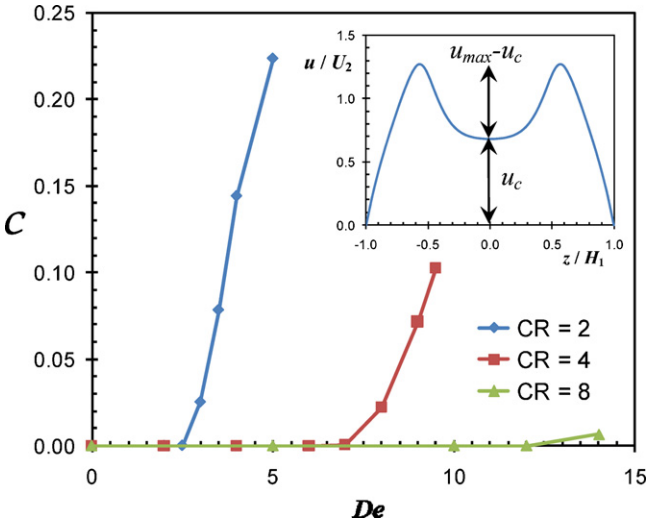

Fig. 8. Quantification of the "cat's ears" effect (cf. Eq. (5) for C definition) as a function of the Deborah number for geometries of different contraction ratio (UCM fluid at $Re = 0$).

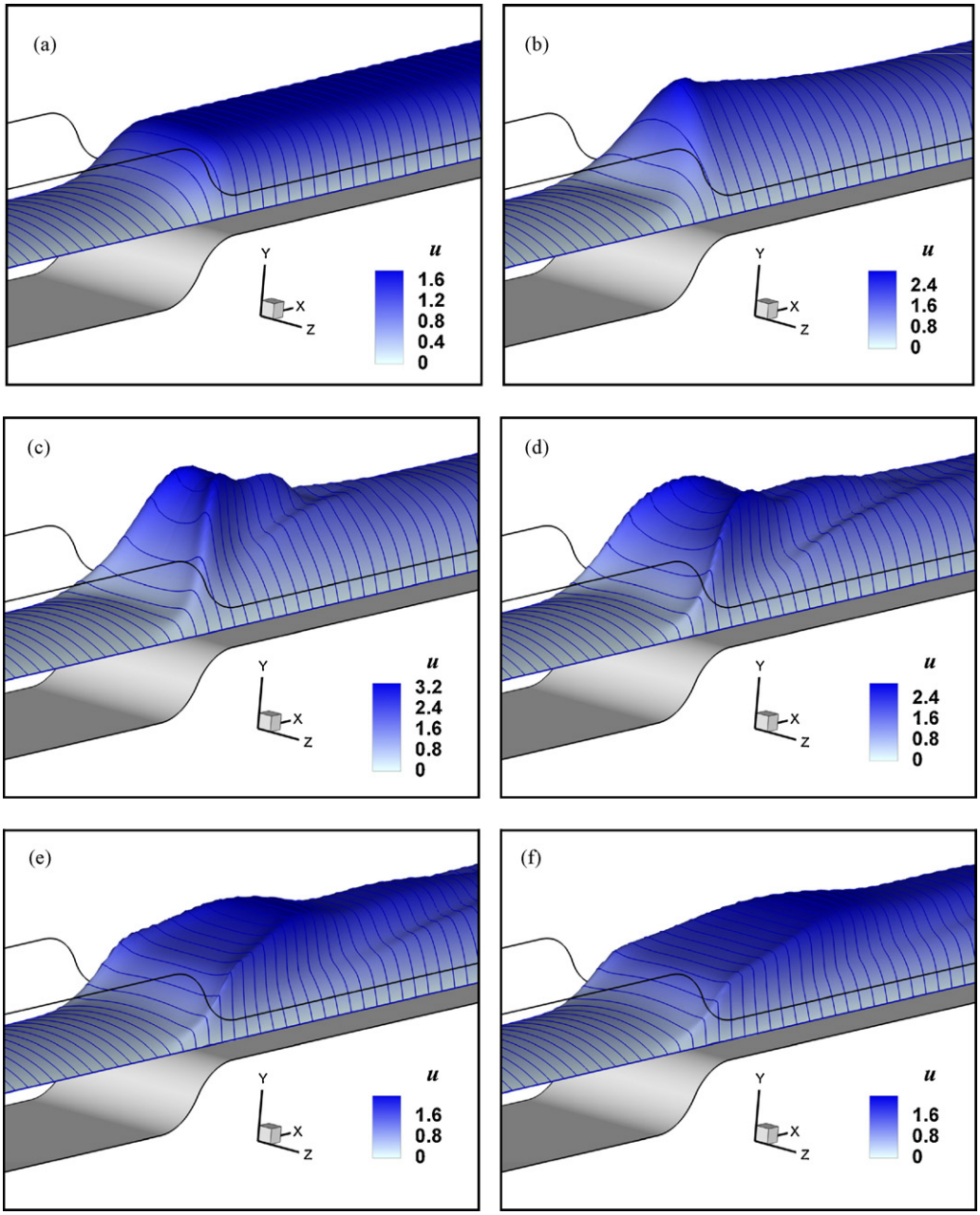

Fig. 9. Influence of the Reynolds number on the streamwise velocity profiles in the *XZ* centreplane ($y = 0$) for $CR = 4$ and $De = 6$ using the UCM model. (a) $Re = 0$, (b) $Re = 0.5$, (c) $Re = 1$, (d) $Re = 2$, (e) $Re = 5$, and (f) $Re = 10$.

We shall focus our attention on the central *XZ* plane ($y = 0$), as this is the plane where the "cat's ears" are observed. In Fig. 11(a) and (b) we plot the stream traces at the centreplane, for $CR = 2$, to illustrate the difference between the Newtonian case (a), and a high Deborah number flow (b), where the "cat's ears" are present. We superimpose the contours of dimensionless pressure, $(p - p_{ref})/(\eta U_2/H_2)$, in order to better illustrate the coupling between the stream traces and the pressure field. The reference pressure was chosen at $x/H_2 = -5$ ($y = z = 0$). The stream traces are aligned with the *x*-direction in the Newtonian case, a result that is compatible with the absence of velocity overshoots along the *spanwise* (neutral) direction. In contrast for the viscoelastic case we observe a significant deviation of the stream traces in this plane especially in the contraction region (the beginning and the end of the contraction are marked with arrows in Fig. 11), and the pressure field is found to be the main driving force for the deviation of the stream traces. To better illustrate this finding, in Fig. 12 we plot the streamwise pressure profiles along the centreline ($y = z = 0$) and along the *z*-plane channel wall ($y = 0$; $z/H_1 = 1$). For the Newtonian case there is no visible difference between the pressure profiles, as anticipated from Fig. 11, thus the driving force for flow is the pressure gradient along the *x*-direction, and therefore the flow in the *XZ* centreplane is nearly unidirectional. For the viscoelastic case close to the end of the contraction region we observe a significant pressure recovery near the sidewall (point C, cf. Fig. 11) and this non-negligible pressure gradient along the spanwise direction (C–D) leads to a bending of the stream traces towards the centreline. This partly elucidates the large velocity overshoots on the centreline that emerge at high *De*, for all *CR* as shown in Figs. 6(b) and 7(b).

Along the centreline the flow is extensionally dominated, and the analysis presented by Alves and Poole [10] for UCM fluid flow in smooth planar contractions is useful. In Ref. [10] it was shown

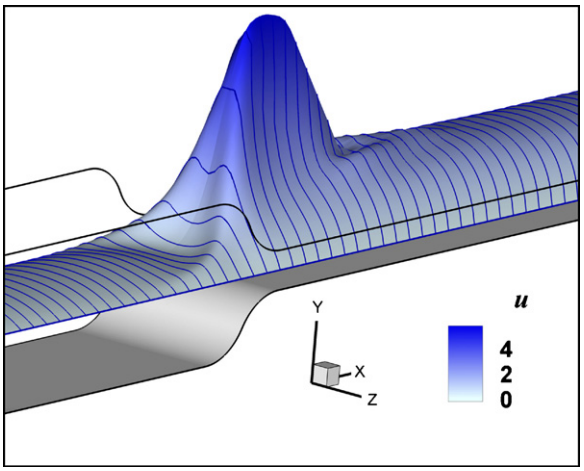

Fig. 10. Streamwise velocity profiles in the *XZ* centreplane ($y = 0$) for $CR = 4$, using the PTT model with $\varepsilon = 0.02$, at $De = 16$ and $Re = 0.5$.

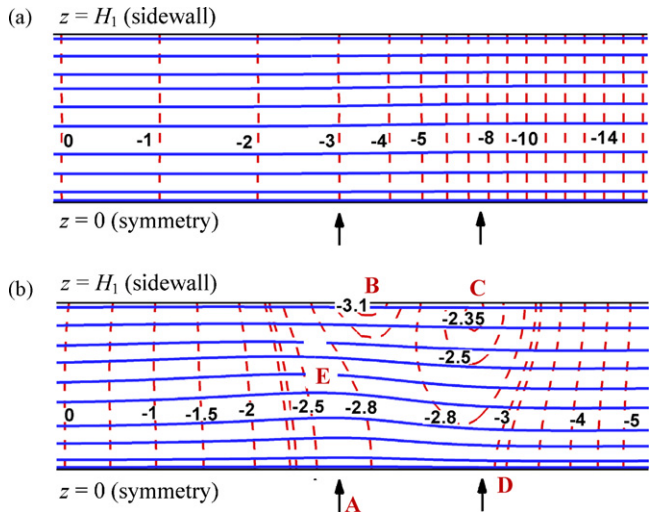

Fig. 11. Stream traces and dimensionless pressure contours of $(p - p_{ref})/(\eta U_2/H_2)$ on the *XZ* centreplane ($y = 0$) for $CR = 2$ and (a) Newtonian fluid at $Re = 0$; (b) UCM fluid at $De = 5$ and $Re = 0$. The reference value of pressure, p_{ref}, was chosen at $x/H_2 = -5$ ($y = z = 0$). Arrows indicate start and end of contraction.

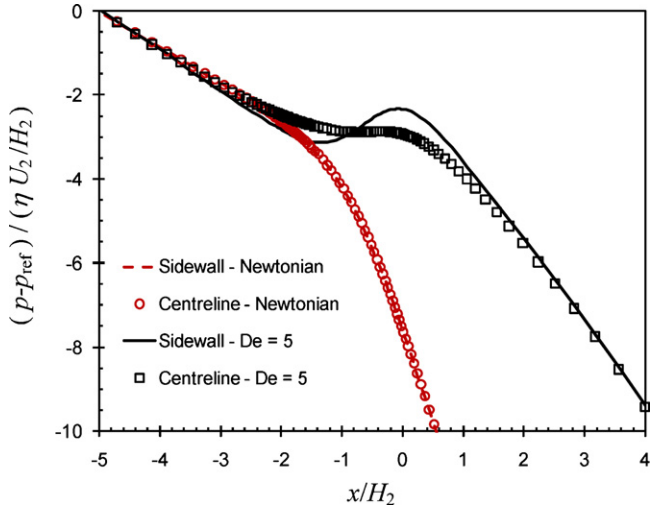

Fig. 12. Pressure profiles along the centreline and near the wall ($y = 0$) for the UCM model under creeping-flow conditions for $CR = 2$. Comparison between Newtonian fluid and $De = 5$ results.

that for two-dimensional contractions strong velocity undershoots along the centreline were observed for highly elastic flows at low *CR*. The existence of these velocity undershoots at the entrance of the contraction region lead to the onset of diverging streamlines, in which the flow moves away from the centreline in a converging region (*XY* plane), where a converging flow would be expected (see, e.g. Ref. [18]). As described in Ref. [10] the existence of strong velocity undershoots and the corresponding diverging flow in smooth contractions is enhanced for low *CR*, and was correlated to the existence of a maximum of the transient Trouton ratio curve that can be estimated for a contraction flow in which the fluid experiences a finite extension, $\varepsilon_H = \ln(CR)$. Incidentally, our numerical simulations suggest that there is a strong correlation between the onset of strong diverging streamlines (in the *XY* plane) and strong velocity overshoots observed in the *XZ* plane (i.e. "cat's ears"). Indeed the stream traces in the *XZ* centreplane ($y = 0$), shown in Fig. 11, exhibit a similar behaviour to the diverging-flow phenomenon. For the sake of simplicity, in what follows we assume that the unidirectional flow in the centreplane observed at low *De* and low *CR* would still be valid for high *De* number flows (which we already know is not the case, as shown in Fig. 11). In this idealised case, the flow at each *z* plane near the centreline (i.e. for small *z*) would behave as a two-dimensional smooth contraction flow, in essence the flow analysed by Alves and Poole [10]. Since at the plane $z = 0$ the velocities are higher, then locally the effective Deborah number at that plane would be a maximum, and we would expect the velocity undershoot to be stronger. In the region where the velocity undershoot is maximum, one expects that the flow will diverge (from continuity), both in the *y* and *z* directions, thus confirming the strong link between diverging streamlines in the *XY* and *XZ* planes and why the observed stream traces behave as those illustrated in Fig. 11(b) for high *De* and low *CR*. As demonstrated in Ref. [10], the diverging flow that occurs at the entrance of the contraction region ensures that near the end of the contraction, where the shear and normal stresses are greatest near the wall, the flow converges towards the centre, thus reducing locally the shear rate at the curved walls with the benefit of reducing the energy dissipation. Although this will lead to a significant increase of the strain rate on the centreline, it does not lead to a significant increase of the normal stresses at the centreline for low *CR* (indeed, as demonstrated in Ref. [10], for low *CR* increasing the strain rate leads to a *decrease* of the Trouton ratio estimated at a characteristic strain $\varepsilon_H = \ln[CR]$). The previous arguments confirm the flow behaviour observed on the *XZ* centreplane for low *CR*, as illustrated in Fig. 11. Between points A and E illustrated in Fig. 11, the streamwise velocity undershoot progressively decreases. On the other hand, near point E in the *XZ* plane stream traces are converging, thus a local velocity maximum (as compared to along the *z* direction at a fixed *x*-position) is observed, generating the surprising "cat's ears" velocity profiles.

6. Conclusions

We have conducted a systematic numerical study of viscoelastic flow, modelled using both the UCM and PTT models, through three-dimensional gradual planar contractions with the aim of simulating the experimentally observed "cat's ears" effect [1–3]. We have been able to reproduce the phenomenon using the UCM model, even for creeping-flow conditions, and our results thus show that neither inertia, shear-thinning shear viscosity nor a second-normal-stress difference are required for these extreme velocity overshoots to occur. Inertia, up to a certain level at least, and the inclusion of shear-thinning effects was seen to enhance the phenomenon.

Guided by the numerical simulations we describe a simple mechanism for the occurrence of the velocity overshoots and how these relate to the diverging flow behaviour typical of highly elastic flows in smooth contractions with small contraction ratios.

Acknowledgements

The authors would like to thank the British Council/Conselho de Reitores das Universidades Portuguesas for support through the 'Treaty of Windsor Programme' (Acção n B-11/07). MAA acknowledges funding by Fundação para a Ciência e a Tecnologia (FCT, Portugal) under projects PTDC/EQU-FTT/71800/2006 and REEQ/928/EME/2005. An illuminating roundtable discussion between the authors, Professor Radhakrishna "Suresh" Sureshkumar (University of Washington St Louis), Dr. Alexander Morozov (University of Edinburgh) and Professor Fernando Pinho (University of Porto) helped in the formulation of the ideas outlined in Section 5 and is here gratefully acknowledged. The valuable suggestions of the anonymous Referees are also gratefully acknowledged.

References

[1] R.J. Poole, M.P. Escudier, P.J. Oliveira, Laminar flow of a viscoelastic shear-thinning liquid through a plane sudden expansion preceded by a gradual contraction, Proc. Roy. Soc. Lond. Ser. A 461 (2005) 3827.
[2] R.J. Poole, M.P. Escudier, A. Afonso, F.T. Pinho, Laminar flow of a viscoelastic shear-thinning liquid over a backward-facing step preceded by a gradual contraction, Phys. Fluids 19 (2007) 093101.
[3] F.L. Keegan, M.P. Escudier, M.A. Alves, R.J. Poole, Viscoelastic flow through gradual contractions: experiments and simulations, in: A. Co, L.G. Leal, R.H. Colby, A.J. Giacomin (Eds.), 15th International Congress on Rheology/80th Annual Meeting of the Society of Rheology. AIP Conference Proceedings, Vol. 1027, 2008, pp. 228–230.
[4] N. Phan-Thien, R.I. Tanner, A new constitutive equation derived from network theory, J. Non-Newt. Fluid Mech. 2 (1977) 353.
[5] A. Afonso, F.T. Pinho, Numerical investigation of the velocity overshoots in the flow of viscoelastic fluids inside a smooth contraction, J. Non-Newt. Fluid Mech. 139 (2006) 1.
[6] J.G. Oldroyd, On the formulation of rheological equations of state, Proc. Roy. Soc. Lond. A 200 (1950) 523.
[7] P.J. Oliveira, F.T. Pinho, G.A. Pinto, Numerical simulation of non-linear elastic flows with a general collocated finite-volume method, J. Non-Newt. Fluid Mech. 79 (1998) 1.
[8] P.J. Oliveira, On the numerical implementation of non-linear viscoelastic models in a finite-volume method, Numer. Heat Trans. B 40 (2001) 283.
[9] M.A. Alves, P.J. Oliveira, F.T. Pinho, Benchmark solutions for the flow of Oldroyd-B and PTT fluids in planar contractions, J. Non-Newt. Fluid Mech. 110 (2003) 45.
[10] M.A. Alves, R.J. Poole, Divergent flow in contractions, J. Non-Newt. Fluid Mech. 144 (2007) 140.
[11] R.D. Mehta, P. Bradshaw, Design rules for small low-speed wind tunnels, Aero. J. (Roy. Aeronaut. Soc.) 83 (1979) 443.
[12] C.J. Doolan, Numerical evaluation of contemporary low speed wind tunnel contraction designs, J. Fluids Eng. 129 (2007) 1241.
[13] A.G. Darbyshire, T. Mullin, Transition to turbulence in constant-mass-flux pipe flow, J. Fluid Mech. 289 (1995) 83.
[14] J.M.J. den Toonder, M.A. Hulsen, G.D.C. Kuiken, F.T.M. Nieuwstadt, Drag reduction by polymer additives in a turbulent pipe flow: numerical and laboratory experiments, J. Fluid Mech. 337 (1997) 193–231.
[15] R.J. Poole, M.P. Escudier, Turbulent flow of viscoelastic liquids through an axisymmetric sudden expansion, J. Non-Newt. Fluid Mech. 117 (2004) 25.
[16] F. Durst, S. Ray, B. Unsal, O.A. Bayoumi, The development lengths of laminar pipe and channel flows, J. Fluids Eng. 127 (2005) 1154.
[17] R.J. Poole, M.A. Alves, P.J. Oliveira, F.T. Pinho, Plane sudden expansion flows of viscoelastic liquids, J. Non-Newt. Fluid Mech. 146 (2007) 79.
[18] D.V. Boger, K. Walters, Rheological Phenomena in Focus, Elsevier, Amsterdam, 1993.